

Supporting Information

Redox-Copolymers for the Recovery of Rare Earth Elements by Electrochemically Regenerated Ion-Exchange

Haley Vapnik,[‡] Johannes Elbert [‡] and Xiao Su ^{*a}

^a Department of Chemical and Biomolecular Engineering, University of Illinois at Urbana-Champaign, Urbana, Illinois 61801, United States.

***Corresponding Author E-mail:** x2su@illinois.edu

Author Contributions: ‡H.V. and J.E. contributed equally.

Contents

SI-1. Materials and instruments	3
SI-2. Preparation of secondary and control adsorbent materials and electrodes	3
SI-3. Stability of P(FPMAM-co-MAA)-CNT electrodes relating to amount of used cross-linker	5
SI-4. Adsorption data fitting by kinetic models	6
SI-5. Adsorption data fitting by isotherm models	8
SI-6. P(FPMAM-co-MAA) adsorbed REE mol to adsorption site ratio calculations	10
SI-7. Scanning electron microscopy (SEM) images and Energy-dispersive X-ray spectroscopy (EDS) mapping	11
SI-8. X-ray photoelectron spectroscopy (XPS) for P(FPMAM-co-MAA) and P(FPMAM-co-MAA)-CNT electrodes	14
SI-9. HR-ESI-MS spectra	15
SI-10. NMR spectra	17
SI-11. P(FPMAM-co-MAA)-CNT electrode cycling: Reduction during uptake stage	22
SI-12. P(FPMAM-co-MAA)-CNT electrode desorption energy consumption	23
SI-13. Gel Permeation Chromatography (GPC)	24
SI-14. Dynamic Light Scattering	24
SI-15. Effect of ionic strength on adsorption	26
SI-16. Adsorption of Y from water using different adsorbents	26
SI-17. Adsorption concentration changes	27
SI-18. P(FPMAM-co-MAA)-CNT electrode solution pH changes	27
SI-19. P(FPMAM-co-MAA)-CNT electrode distribution coefficient	27
References	29

SI-1. Materials and instruments

All chemicals were obtained from Sigma Aldrich, VWR, Fisher Scientific or TCI, and used as received. Hydrogen was received from Airgas. MEHQ was removed from methacrylic acid and BzMA by passing it through a column filled with basic aluminium oxide. 1,3-Benzenedisulfonyl azide (1,3-BDSA) was synthesized according to literature protocols.¹ NMR spectra were recorded on Varian Unity Inova 400 MHz spectrometer or a Varian Unity Inova 500 MHz spectrometer, both equipped with a Nalorac QUAD probe. Electrospray-ionization mass spectrometry (ESI-MS) was performed with a Waters Q-TOF Ultima ESI.

Samples for elemental analysis were weighed with a Mettler Toledo UMT2 and analysed with an Exeter Analytical - Model CE440 CHN Analyser. Scanning Electron Microscopy (SEM) and Energy-dispersive X-ray spectroscopy (EDS) were carried out in the Frederick Seitz Materials Research Laboratory Central Research Facilities, University of Illinois. SEM was taken using a Hitachi S-4700 instrument. Micrograph images were taken at an accelerating voltage of 10 kV. EDS was taken using an attached iXRF EDS Elemental Analysis System with Oxford Instruments (Si(Li) detector). EDS mapping and spectra were taken using an accelerating voltage of 20 kV. The chemical states of iron and presence of REEs on the electrodes were characterized using X-ray photoelectron spectroscopy (XPS; Kratos Axis ULTRA) with monochromatic Al K α X-ray source (210 W). The XPS results were analysed using CASA XPS software (UIUC license). The spectra were fitted into their components following subtraction of a Shirley background from the region of interest. Parameters for curve-fitting of Fe2p were determined from reported literature.^{2,3}

Dynamic light scattering (DLS) was measured using a Malvern Zetasizer ZS using a 633 nm laser. Gel permeation chromatography was measured using a Tosoh EcoSEC 8320 GPC System. Two Tosoh Alpha-M column were used. 14.5 mM LiBr in DMF was used as the mobile phase. The system was calibrated with a poly(methyl methacrylate) (PMMA) standard for relative molar mass estimations. Differential Scanning Calorimetry (DSC) was measured with a Discovery 2500 Differential Scanning Calorimeter at a heating rate of 10 K/min. Thermogravimetric Analysis (TGA) was measured using a Q50 thermogravimetric analyser from TA instruments.

All electrochemical studies were performed on a VersaSTAT 3 or VersaSTAT 4 potentiostat (Princeton Applied Research) using a BASi cell in a three-electrode configuration with an aqueous Ag/AgCl reference electrode, and a Pt counter electrode. The initial and final concentrations of the REE solutions were determined using ICP-OES (5110 ICP-OES, Agilent Technologies). Samples were diluted with 2% nitric acid (except for Ce samples which required 5% nitric acid) and were ran through the ICP in 10 replicates, with each experiment solution repeated in triplicates and each experiment repeated at least twice. The wavelengths used were Y 371.029nm, Nd 470.654nm, Dy 353.171nm, Gd 336.224nm, Eu 263.877nm, and Ce 418.659nm.

SI-2. Preparation of secondary and control adsorbent materials and electrodes

Preparation of P(FPMAM-co-MAA)-CNT Electrodes with varied amounts of crosslinking. Two stocks were prepared: stock A of 12 mg of P(FPMAM-co-MAA) (P1) in 3 mL of Deionized (DI) water and 60 μ L of 1M NaOH, and stock B with 12 mg of CNT (multiwalled carbon nanotubes, Sigma-Aldrich) and varied amounts of cross-linker in 1.5 mL of Dimethylformamide (DMF). Added cross-linker percentage to mass: 0% cross-linker 0 mg cross-linker, 5% cross-linker 0.6 mg cross-linker, 10% cross-linker 1.2 mg cross-linker, 20% cross-linker 2.4 mg cross-linker. Stock A solution was stirred and heated until polymer was fully dissolved while stock B was sonicated for 30 min. in icy water. The P1/CNT (1:1) ratio was prepared by mixing stocks A and B and sonicated for 4 h in an ice-bath. Once prepared, Titanium-grade 1 mesh (titanium screen, Fuel Cell Store) cut into rectangles (1 cm \times 2 cm, 53 μ m thick), were drop-coated by the solution with the active material, with about 40-50 μ L for each drop, and left to dry at 95 $^{\circ}$ C in oven between drops. Coated area was about 1 cm \times 1 cm surface area on each front and back side. After coating, polymer-coated electrodes left overnight to ensure all solvent is

evaporated. Then electrodes left in oven at 140 °C for 3 h to activate crosslinking. Coated electrodes were then connected to a copper wire with copper tape. The same methodology was used for P(FPMAM₇₀-co-MAA₃₀)-CNT Electrodes, P(FPMAM₂₅-co-MAA₇₅)-CNT Electrodes, and Preparation of P(BzMA₅₂-MAA₄₈)-CNT Electrodes.

Preparation of CNT Electrodes. Stock 12 mg of CNT (multiwalled carbon nanotubes, Sigma-Aldrich) dispersed in 3 mL of chloroform (4 mg of CNT/ 1 mL chloroform). Stock solution was sonicated in icy water to allow for CNT dispersion. Once prepared, Titanium-grade 1 mesh (titanium screen, Fuel Cell Store) cut into rectangles (1 cm × 2 cm, 53 μm thick), were dip-coated by the solution with the CNT material. Coated area was about 1 cm × 1 cm surface area on each front and back side. Coated electrodes were then connected to a copper wire with copper tape.

Preparation of FPMAM-CNT Electrodes. Electrode preparation was adapted from previously reported procedures.⁴ Two stocks were prepared: stock A of 40 mg of FPMAM (P4) and 20 mg of CNT in 10 mL of anhydrous chloroform, and stock B with 20 mg of CNT. The two stock solutions were sonicated for 2 h in icy water to optimize dispersion level. The P4/CNT (1:1) ratio was prepared by mixing stocks A and B in a 1:1 ratio and sonicated for another 3 h in an ice-bath. Once prepared, Titanium-grade 1 mesh (titanium screen, Fuel Cell Store) cut into rectangles (1 cm × 2 cm, 53 μm thick), were dip-coated by the solution with the CNT material. Coated area was about 1 cm × 1 cm surface area on each front and back side. Coated electrodes were then connected to a copper wire with copper tape.

SI-3. Stability of P(FPMAm-co-MAA)-CNT electrodes relating to amount of used cross-linker

Cyclic voltammetry (CV) characterization was carried out to investigate the stability, with varying amounts of added cross-linker, of P1-CNT/Ti. Electrodes were placed in 10 mL of 100 mM NaClO₄ aqueous solution with CVs conducted in potential range of -1.1 to 1.1 V for all cycles. Over 100 cycles were conducted for each electrode (5 cycles @ 0.1 V/s → 100 cycles @ 0.05 V/s → 5 cycles @ 0.01 V/s → 11 cycles @ 0.05 V/s). 100 cycles of the CV ran at a scan rate of 0.05 V/s are shown in **Figure S1**.

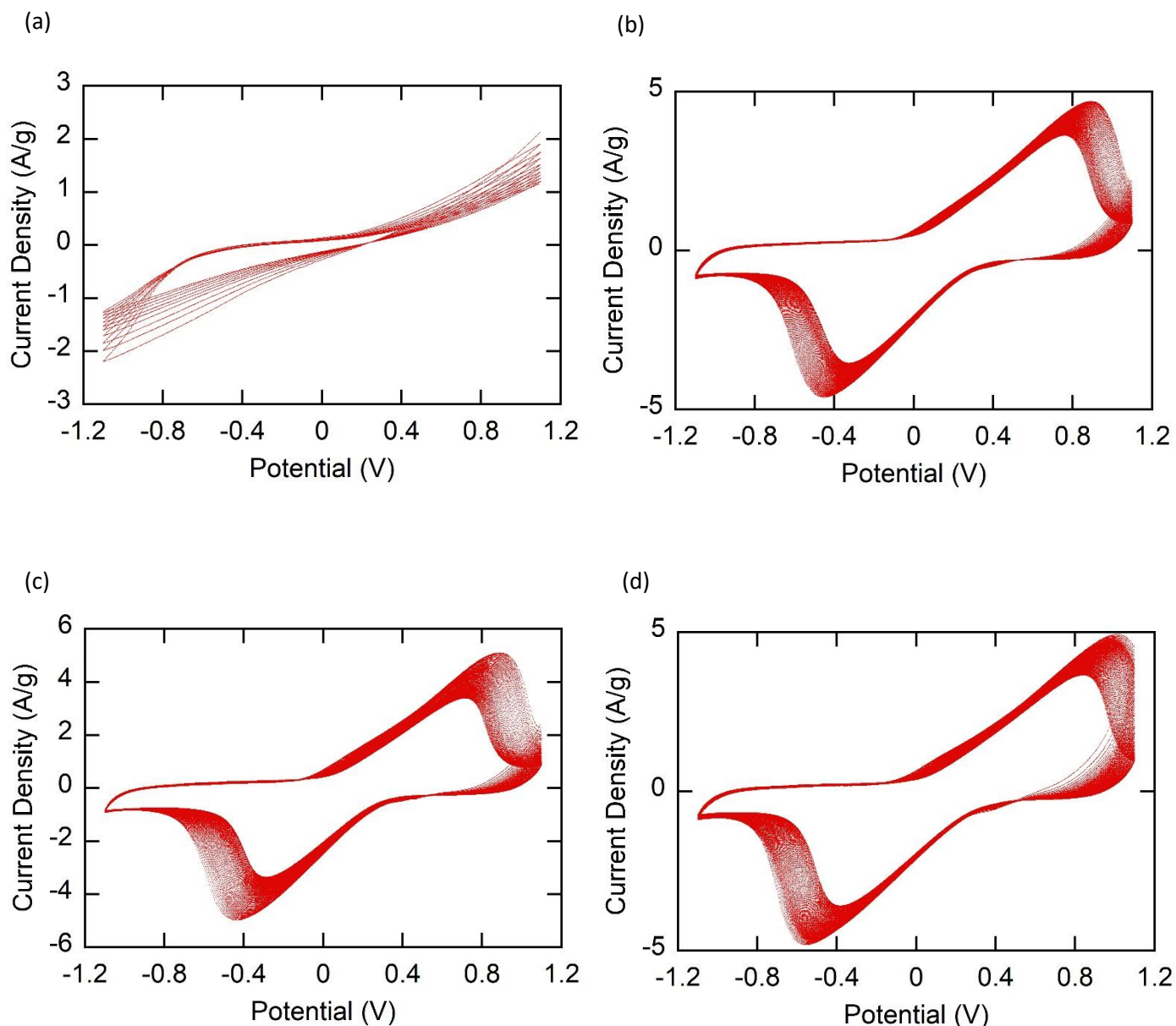


Figure S1. Cyclic voltammetry of P1-CNT/Ti electrodes (with varying amounts of cross-linker) for 100 cycles in the presence of 100 mM NaClO₄. The potential range chose was from -1.1 to 1.1 V with scan rate 50 mV/s. a) P1-CNT/Ti w/ 0% cross-linker. a) P1-CNT/Ti w/ 0% cross-linker. b) P1-CNT/Ti w/ 5% cross-linker. c) P1-CNT/Ti w/ 10% cross-linker. d) P1-CNT/Ti w/ 20% cross-linker.

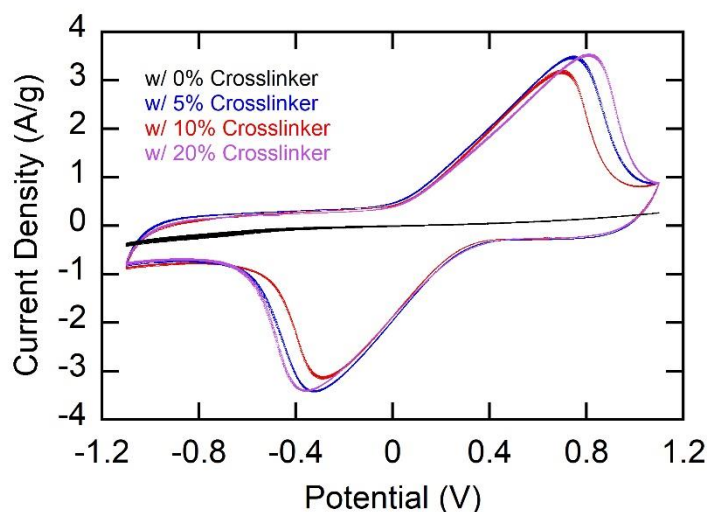


Figure S2. Cyclic voltammetry of P1-CNT/Ti electrodes (with varying amounts of cross-linker) final 10 cycles (from over 100 cycles) in the presence of 100 mM NaClO₄. The potential ranged -1.1 to 1.1 V with a scan rate 50 mV/s.

SI-4. Adsorption data fitting by kinetic models

To investigate the adsorption process of Y(III) on P1-CNT/Ti, pseudo-first-order (PFO) and pseudo-second-order (PSO) kinetic models were used to fit the experimental kinetics data. The linear forms of PFO (eq S1) and PSO (eq S2) models are expressed as follows.^{5, 6}

$$\log(q_e - q_t) = \log q_e - \frac{k_1}{2.303} t \quad (S1)$$

$$\frac{t}{q_t} = \frac{1}{k_2 q_e^2} + \frac{t}{q_e} \quad (S2)$$

Here, q_e and q_t (mg/g) are the amount of Y(III) adsorbed on the adsorbent at equilibrium and at time t (min), respectively. k_1 (min⁻¹) and k_2 (g mg⁻¹ min⁻¹) are the PFO and PSO rate constants, respectively. The slope and intercept of $\log(q_e - q_t)$ vs t are used to determine the rate constant for PFO with a straight line suggesting the applicability of the PFO kinetic model to fit the experimental data. The slope and intercept of t/q_t vs t are used to determine the rate constant for PSO with a linear relationship suggesting if PSO kinetics is. **Figure S3** shows the linear fit plots for both kinetic models and the final fits to the experimental data. The parameters of the PFO and PSO models and the correlation coefficients (R^2) estimated using the two models are given in **Table S1**. **Figure S4** shows the kinetic data and modelling using PFO and PSO for the adsorption Y(III) on P1-CNT/Ti.

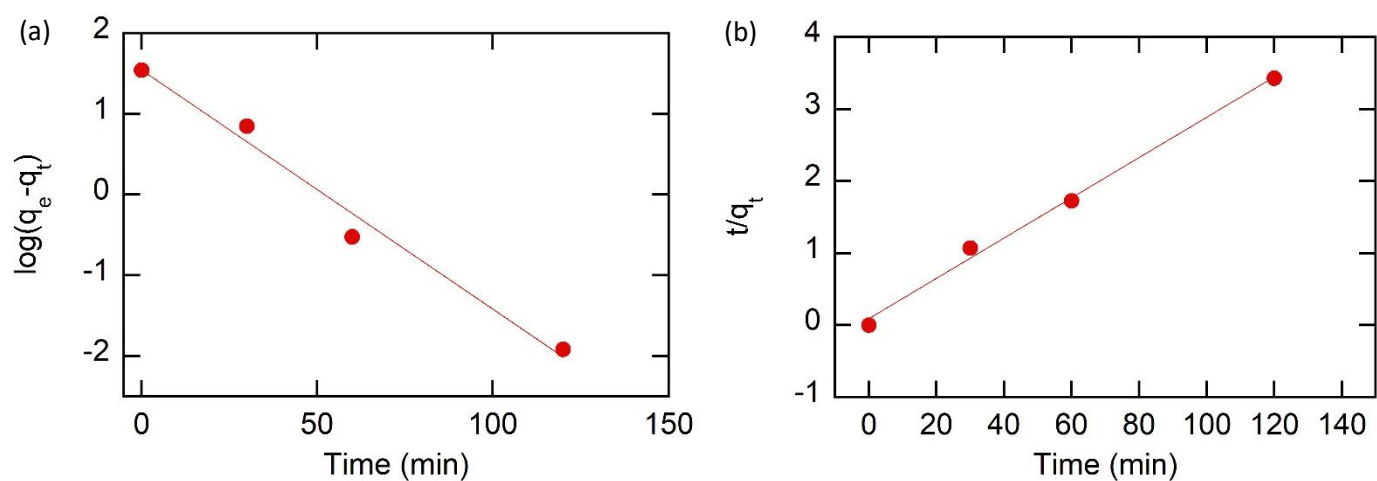


Figure S3. The pseudo-first-order (a) and pseudo-second-order kinetics model (b) plots for Y(III) adsorption on P1-CNT/Ti.

Table S1. Adsorption Kinetic Model Constants for Adsorption of Y(III) on P1-CNT/Ti

Model	Parameters		R ²
pseudo-first-order model	q _e (mg/g)	k ₁ (min ⁻¹)	0.9817
	35.01	0.0682	
pseudo-second-order model	q _e (mg/g)	k ₂ (g mg ⁻¹ min ⁻¹)	0.9951
	35.75	0.0088	

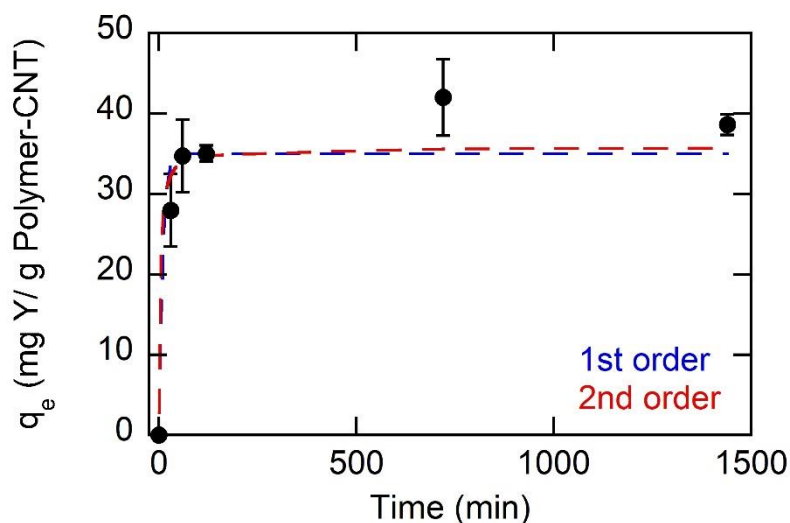


Figure S4. Kinetic data and modelling for the adsorption of Y(III) on P1-CNT/Ti.

SI-5. Adsorption data fitting by isotherm models

The Langmuir isotherm model is given by eq S3:^{7, 8}

$$\frac{C_e}{q_e} = \frac{1}{K_L q_{\max}} + \frac{C_e}{q_{\max}} \quad (S3)$$

C_e (mg/L) represents the equilibrium concentration of Y(III) in the solution, q_e (mg/g) is the amount of Y(III) adsorbed on the adsorbent, q_{\max} (mg/g) is the maximum adsorption capacity of Y(III), and K_L (L/mg) is the Langmuir constant. The experimental data was fitted to the Langmuir model through plotting C_e/q_e versus C_e . The fitted line is used to obtain q_{\max} and K_L from the slope and intercept (**Figure S5a**).

The Freundlich mode is given by:^{8, 9}

$$\ln q_e = \ln K_F + \frac{1}{n} \ln C_e \quad (S4)$$

K_F (mg/g) is a Freundlich equation constant that indicates adsorption capacity and n is the Freundlich constant indicating adsorption intensity. K_F and n are determined from the slope and intercept of the linear plot of $\ln(q_e)$ versus $\ln(C_e)$ (**Figure S5b**).

The parameters of the Langmuir and Freundlich models and the correlation coefficients (R^2) estimated using the two models are given in **Table S2**. **Figure S6** shows the adsorption isotherm and modelling using Langmuir and Freundlich for the adsorption Y(III) on P1-CNT/Ti.

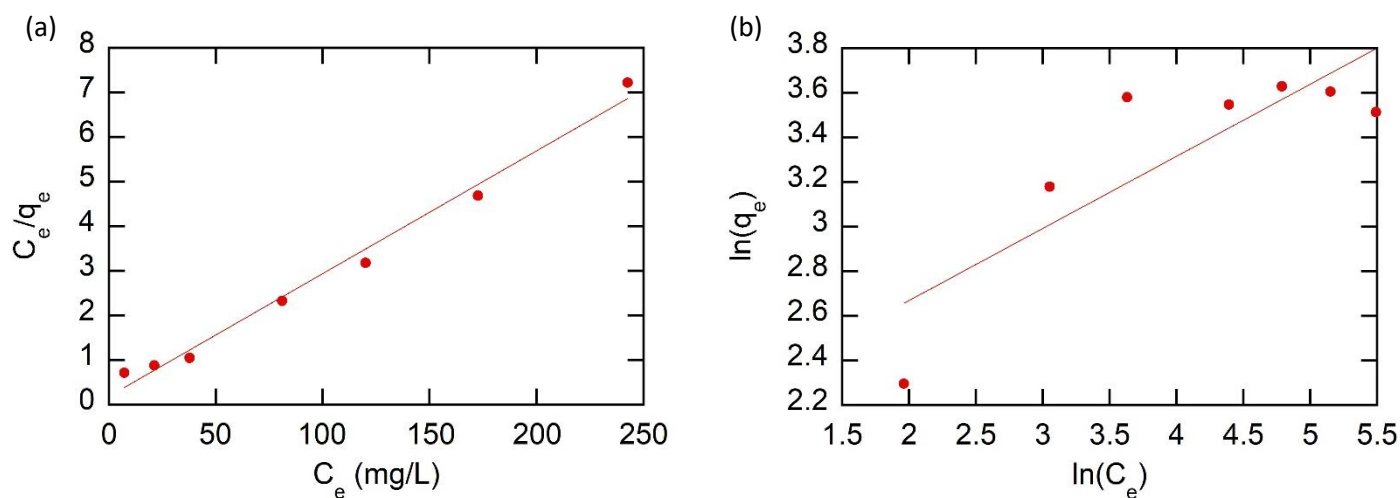


Figure S5. Langmuir isotherm (a) and Freundlich isotherm model (b) plots for Y(III) adsorption on P1-CNT/Ti

Table S2. Adsorption Isotherm Model Constants for Adsorption of Y(III) on P1-CNT/Ti

Isotherm	Parameters		R ²
Langmuir	q_{\max} (mg/g)	K_L (L/mg)	0.9871
	36.35	0.15	
Freundlich	n	K_F (mg/g)	0.7088
	3.09	7.54	

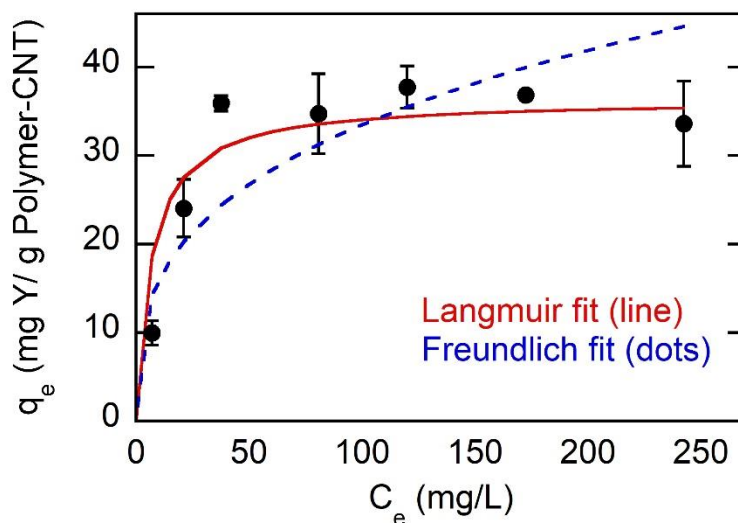


Figure S6. Adsorption isotherm and modeling of Y(III) adsorption on P1-CNT/Ti: Langmuir (line) and Freundlich adsorption isotherm (dots).

SI-6. P(FPMAM-co-MAA) adsorbed REE mol to adsorption site ratio calculations

The number of adsorbed REE moles and moles of adsorption sites (COOH) on the polymer are calculated and compared to give an idea of adsorbent uptake efficiency and the relationship of the adsorption sites the adsorbed RE ions.

m = mass of total electrode coating (mg)

m_p = mass of polymer on electrode (mg)

m_{MAA} = mass of provided by MAA in polymer on electrode (mg)

MW_{COOH} = molecular weight of MAA monomer (g/mol)

$$\text{MW}_{\text{COOH}} = 86.09 \text{ (g/mol)}$$

MW_{Fc} = molecular weight of FPMAM monomer (g/mol)

$$\text{MW}_{\text{Fc}} = 311.2 \text{ (g/mol)}$$

MW_{REE} = molecular weight of REE (g/mol)

C₀ = Initial RE ion concentration in solution (mg/L)

C = Final RE ion concentration in solution (mg/L)

V = Volume of solution (L)

FPMA_{mol%} = mol% of FPMA for given copolymer (mol%)

MAA_{mol%} = mol% of MAA for given copolymer (mol%)

n_{COOH} = moles of MAA (adsorption sites) on given electrode (mmol)

n_{REE} = moles of REE adsorbed onto given electrode (mmol)

Note: Electrode polymer mass (m_p) is estimated to equal half of the total electrode coating (i.e. $m_p = \frac{m}{2}$) since the electrode coating is made with a 1:1 polymer to CNT mix.

Moles of adsorption sites on given adsorbent is calculated as follows:

$$m_{\text{MAA}} = m_p \times \frac{\text{MAA}_{\text{mol}\%} \times \text{MW}_{\text{COOH}}}{(\text{FPMA}_{\text{mol}\%} \times \text{MW}_{\text{Fc}}) + (\text{MAA}_{\text{mol}\%} \times \text{MW}_{\text{COOH}})}$$

$$n_{\text{COOH}} = \frac{m_{\text{MAA}}}{\text{MW}_{\text{COOH}}}$$

Moles of REE ions adsorbed is calculated as follows:

$$n_{\text{REE}} = \frac{C_0 - C}{\text{MW}_{\text{REE}}} \times V$$

SI-7. Scanning electron microscopy (SEM) images and Energy-dispersive X-ray spectroscopy (EDS) mapping

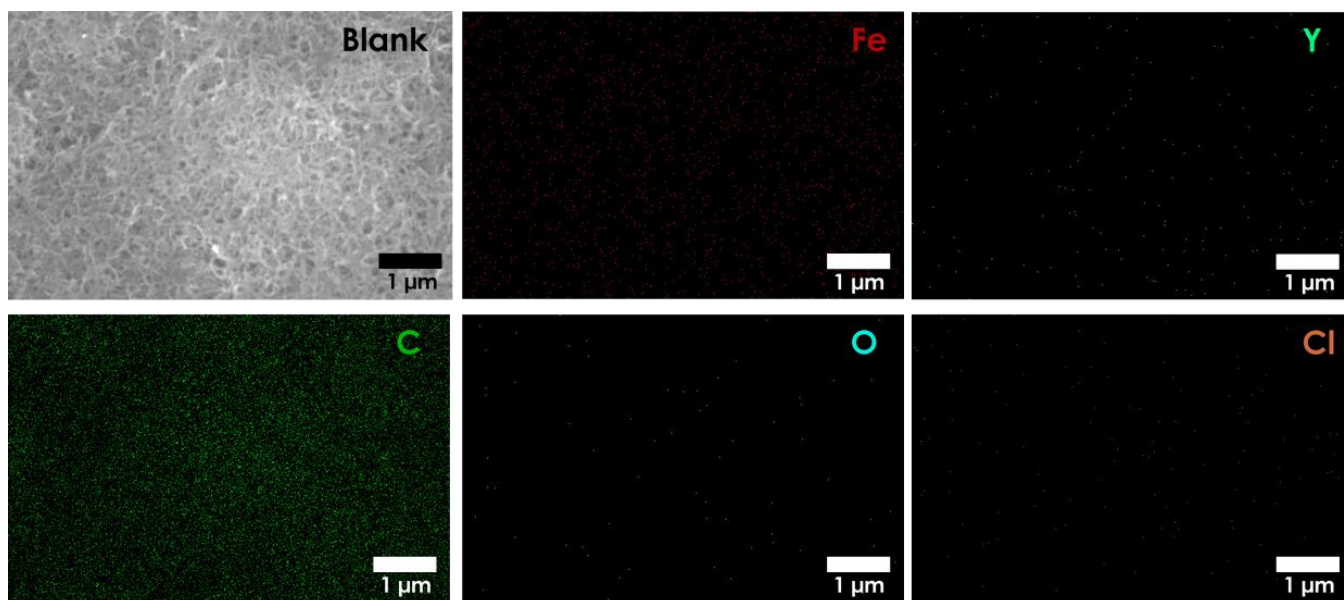


Figure S7. EDS mapping of P1-CNT/Ti electrode, Pristine (Blank).

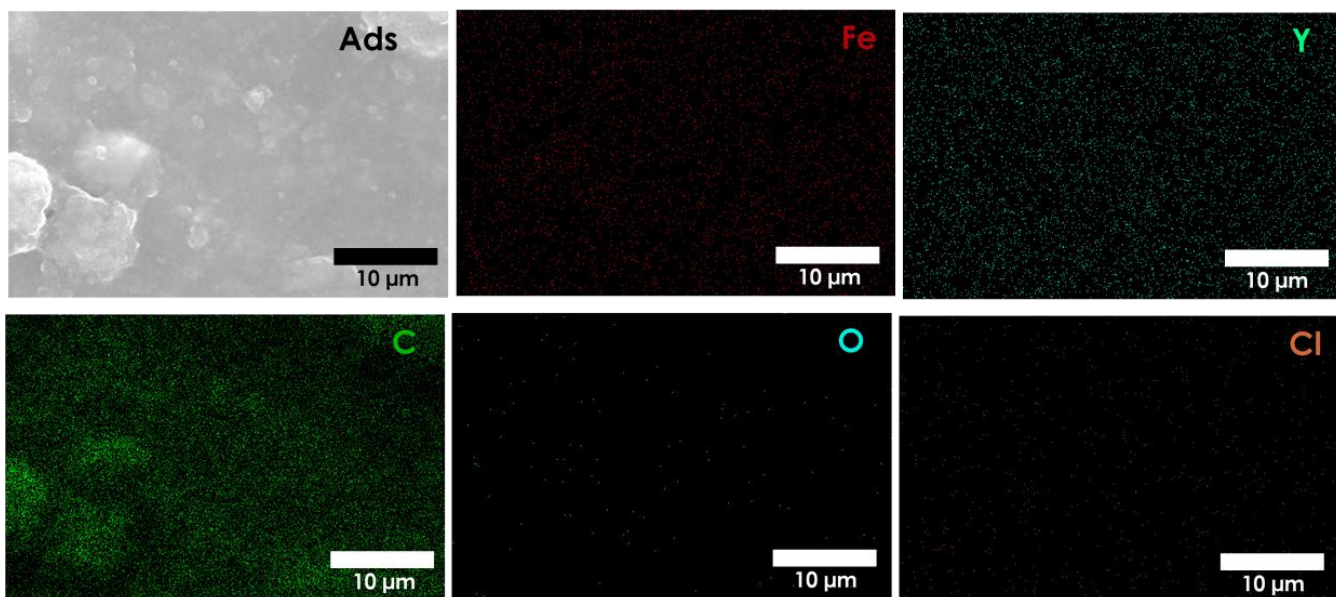


Figure S8. EDS mapping of P1-CNT/Ti electrode after 1 h open circuit Y adsorption.

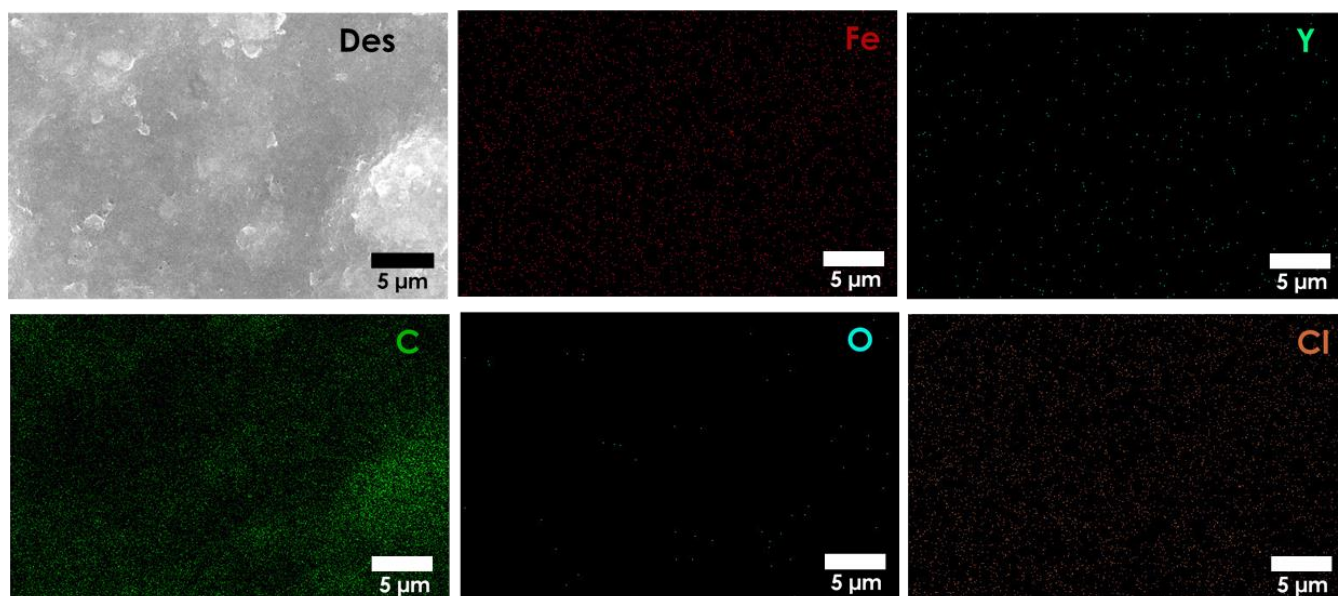


Figure S9. EDS mapping of P1-CNT/Ti electrode after 1 h open circuit Y adsorption then 1 h desorption with applied potential of +0.8 V Ag/AgCl.

Table S3. SEM-EDS analysis of P1-CNT/Ti electrodes (a) Pristine (Blank), (b) After 1 h open circuit Y adsorption, (c) After 1 h open circuit Y adsorption then 1 h desorption with applied potential of +0.8 V Ag/AgCl.

Elt.	Line	Blank (a)		Ads-Y (b)		Des-Y (c)	
		Atomic %	Con wt. %	Atomic %	Con wt. %	Atomic %	Con wt. %
C	Ka	89.151	77.342	92.240	78.022	93.000	80.846
N	Ka	0.000	0.000	0.000	0.000	0.000	0.000
O	Ka	4.298	4.967	3.588	4.043	2.238	2.592
Na	Ka	3.645	6.052	0.267	0.432	0.144	0.239
S	Ka	0.119	0.276	0.052	0.118	0.045	0.103
Cl	Ka	0.051	0.132	0.349	0.870	1.690	4.336
Fe	Ka	2.654	10.706	2.329	9.161	2.787	11.264
Y	La	0.082	0.525	1.174	7.353	0.096	0.619

SI-8. X-ray photoelectron spectroscopy (XPS) for P(FPMAm-co-MAA) and P(FPMAm-co-MAA)-CNT electrodes

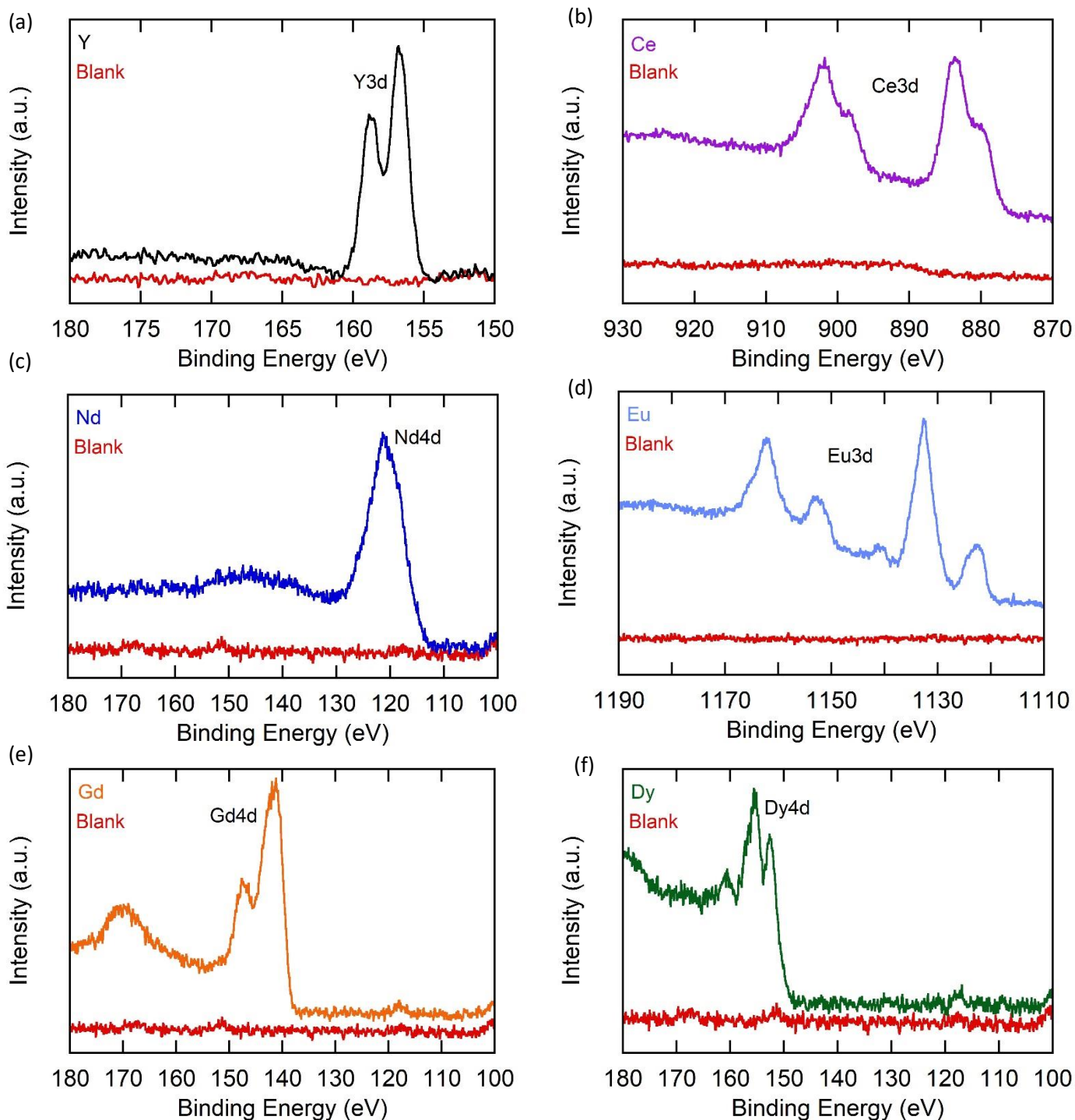


Figure S10. High-resolution XPS spectra of (a) Y_{3d}, (b) Ce_{3d}, (c) Nd_{4d}, (d) Eu_{3d}, (e) Gd_{4d}, and (f) Dy_{4d} before and after adsorption.

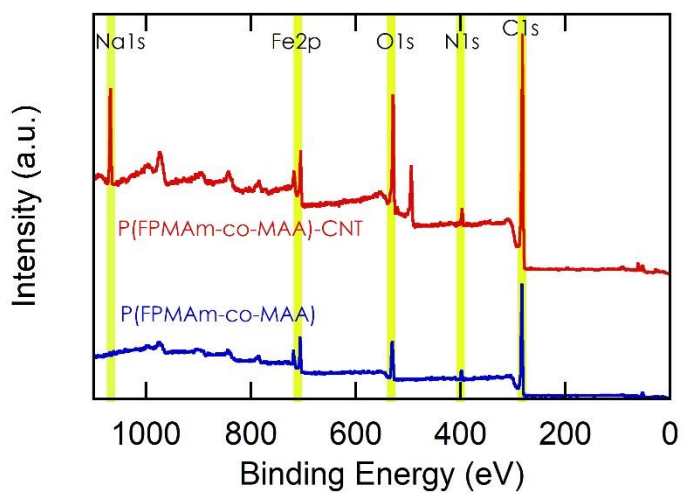


Figure S11. XPS spectra of the polymer P(FPMAM-co-MAA) and the pristine P(FPMAM-co-MAA)-CNT electrode.

SI-9. HR-ESI-MS spectra

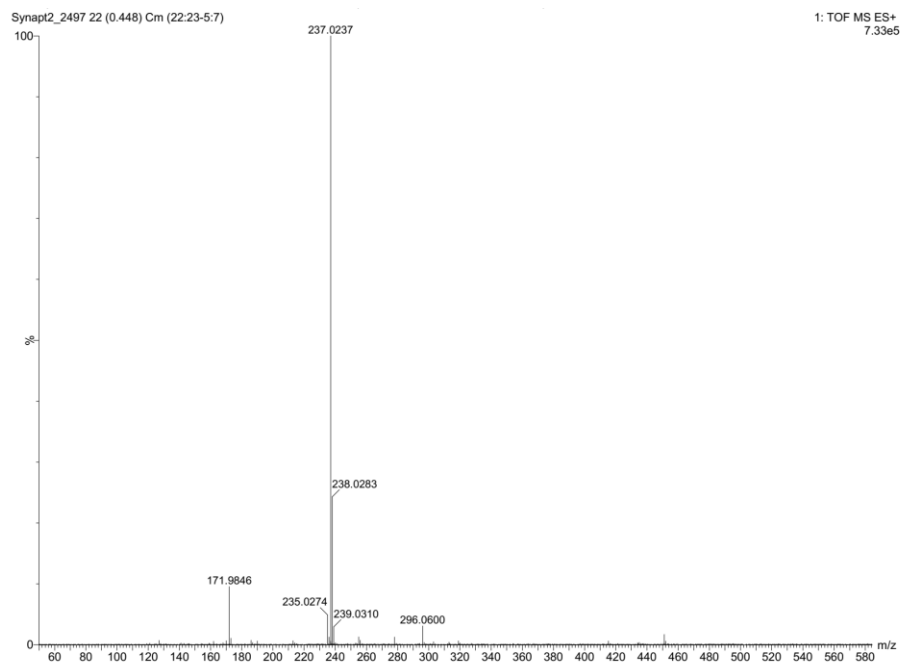


Figure S12. HR-ESI-MS of 2-cyanovinyl ferrocene.

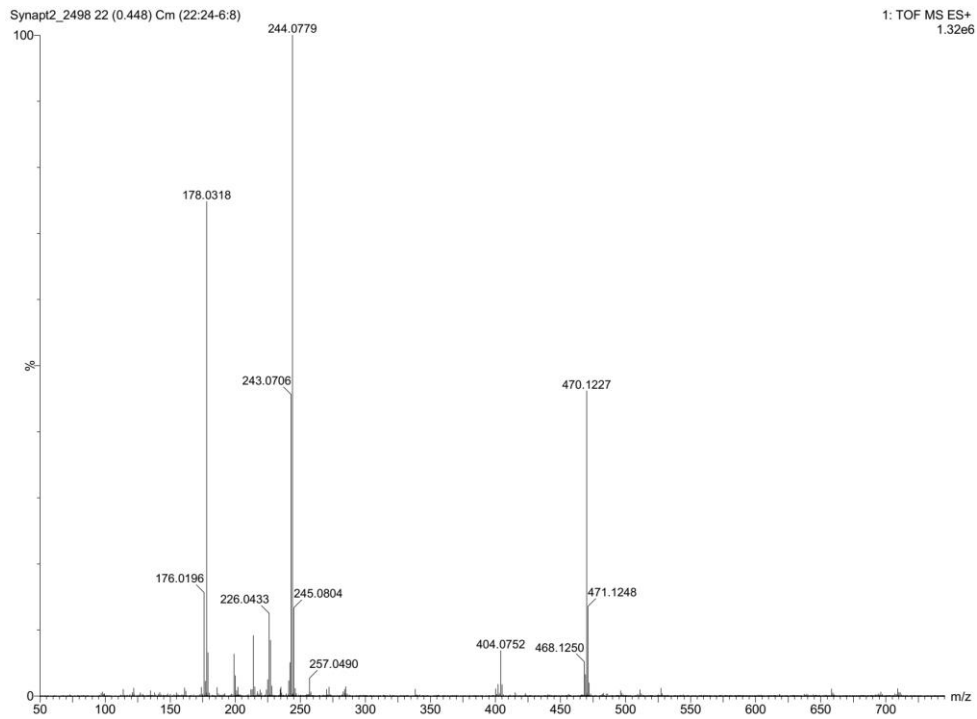


Figure S13. HR-ESI-MS of 3-ferrocenyl propylamine.

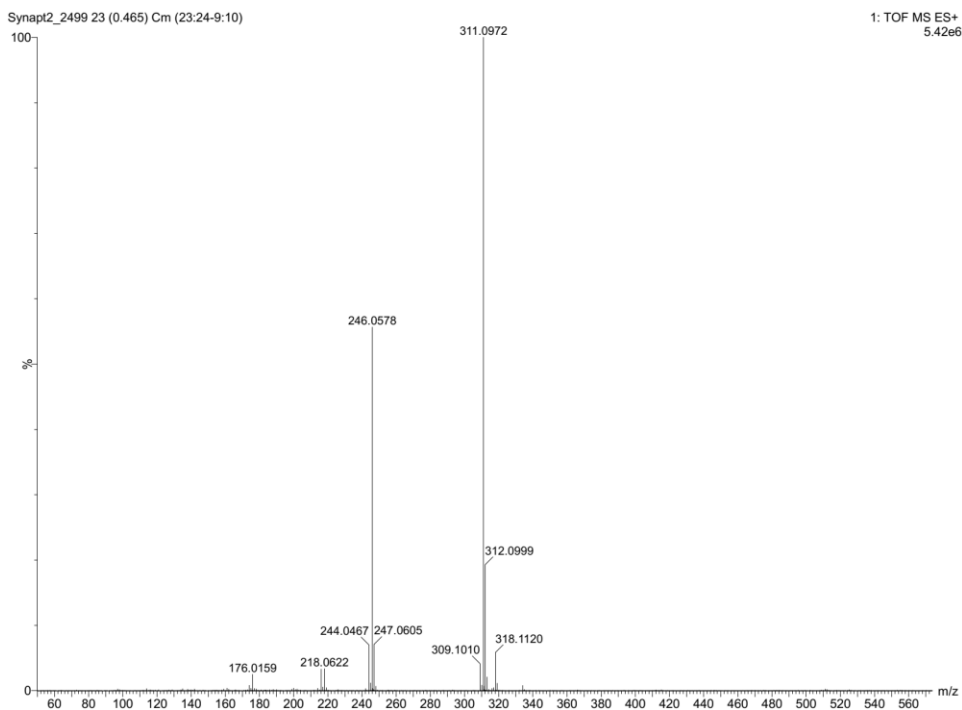


Figure S14. HR-ESI-MS of 3-ferrocenyl propyl methacrylamide (FPMAM).

SI-10. NMR spectra

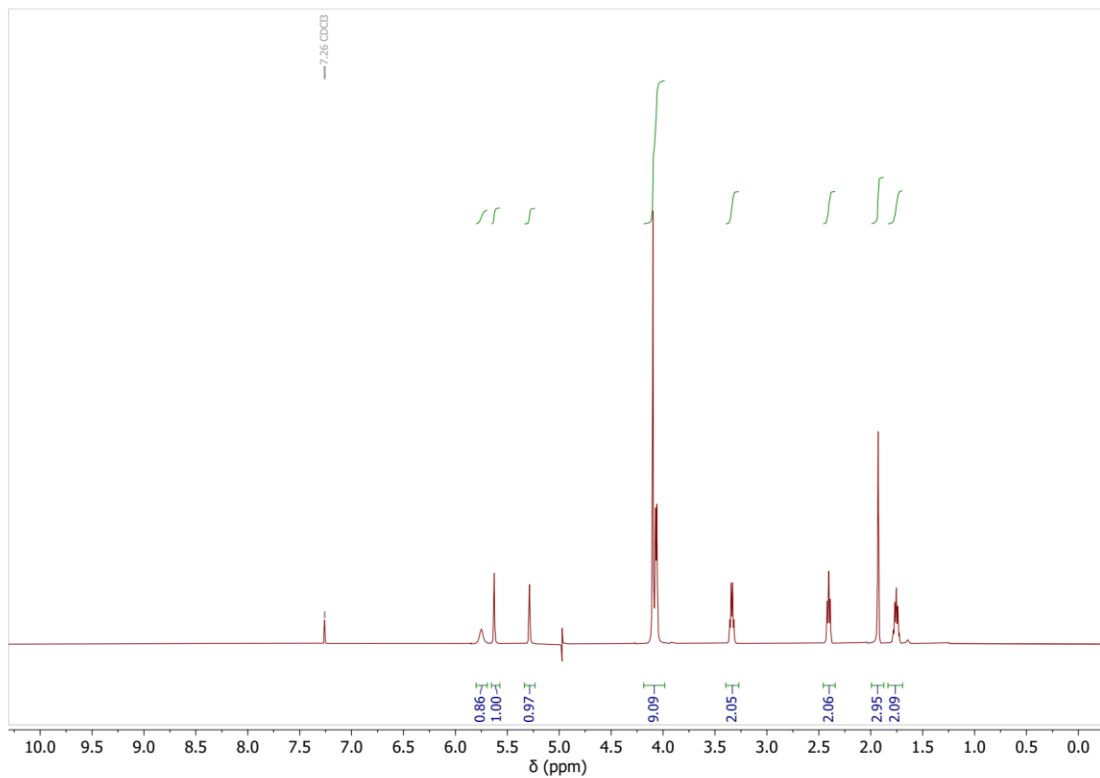


Figure S15. $^1\text{H-NMR}$ spectrum of 2-cyanovinyl ferrocene (500 MHz, CDCl_3).

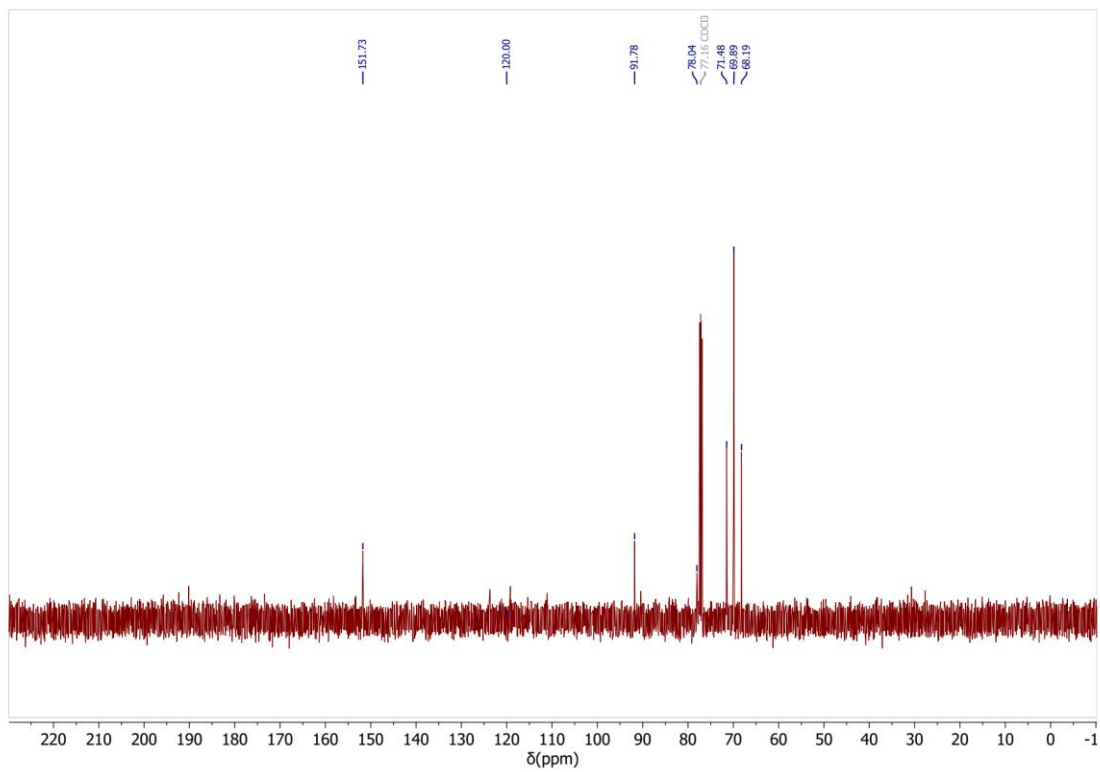


Figure S16. $^{13}\text{C-NMR}$ spectrum of 2-cyanovinyl ferrocene (126 MHz, CDCl_3).

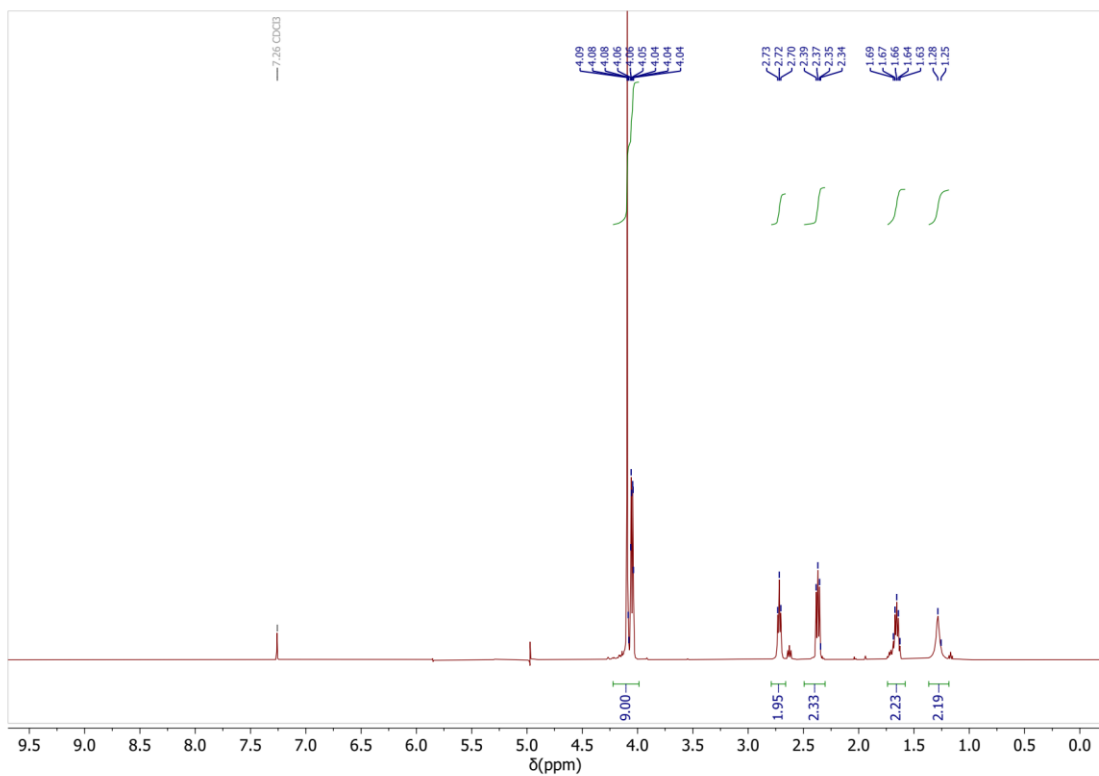


Figure S17. ^1H -NMR spectrum of 3-ferrocenyl propylamine (500 MHz, CDCl_3).

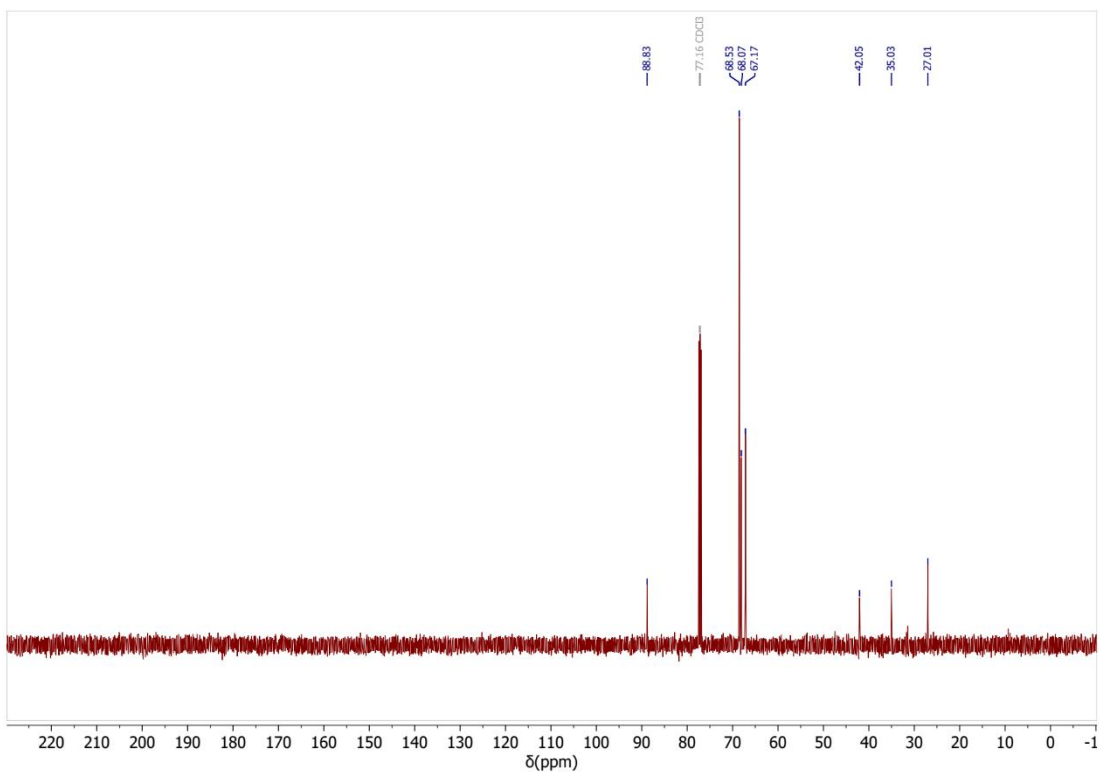


Figure S18. ^{13}C -NMR spectrum of 3-ferrocenyl propylamine (126 MHz, CDCl_3).

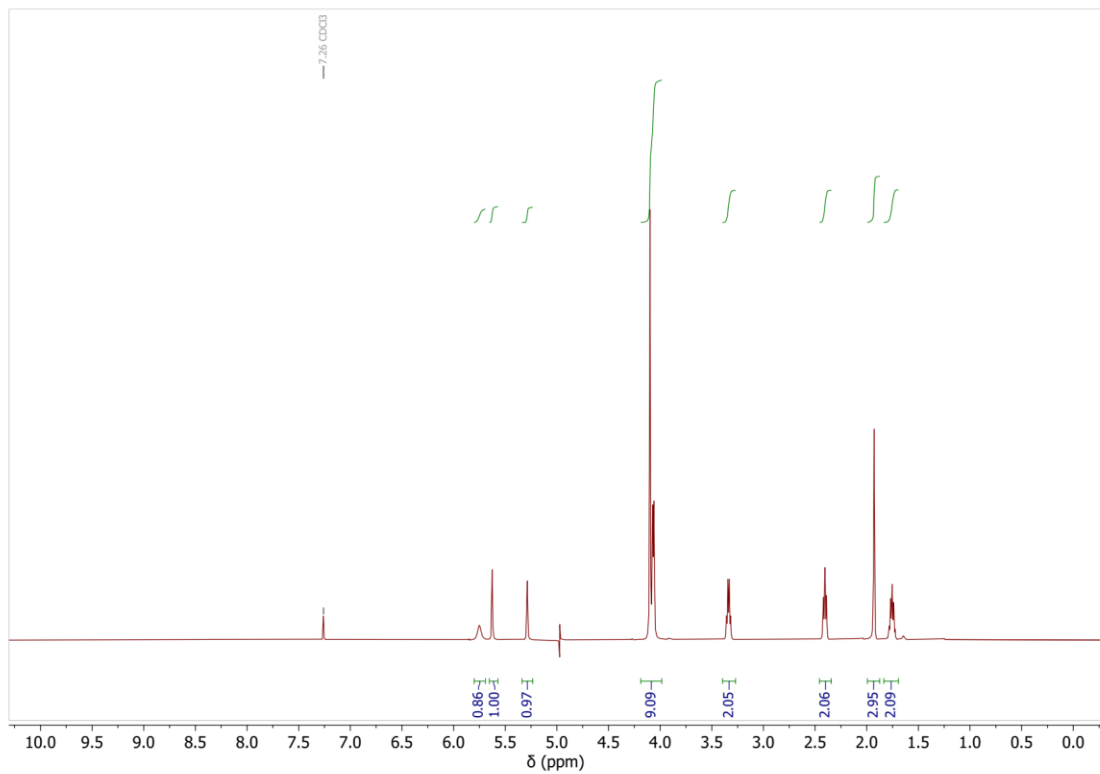


Figure S19. $^1\text{H-NMR}$ spectrum of 3-ferrocenyl propyl methacrylamide (FPMAm) (500 MHz, CDCl_3).

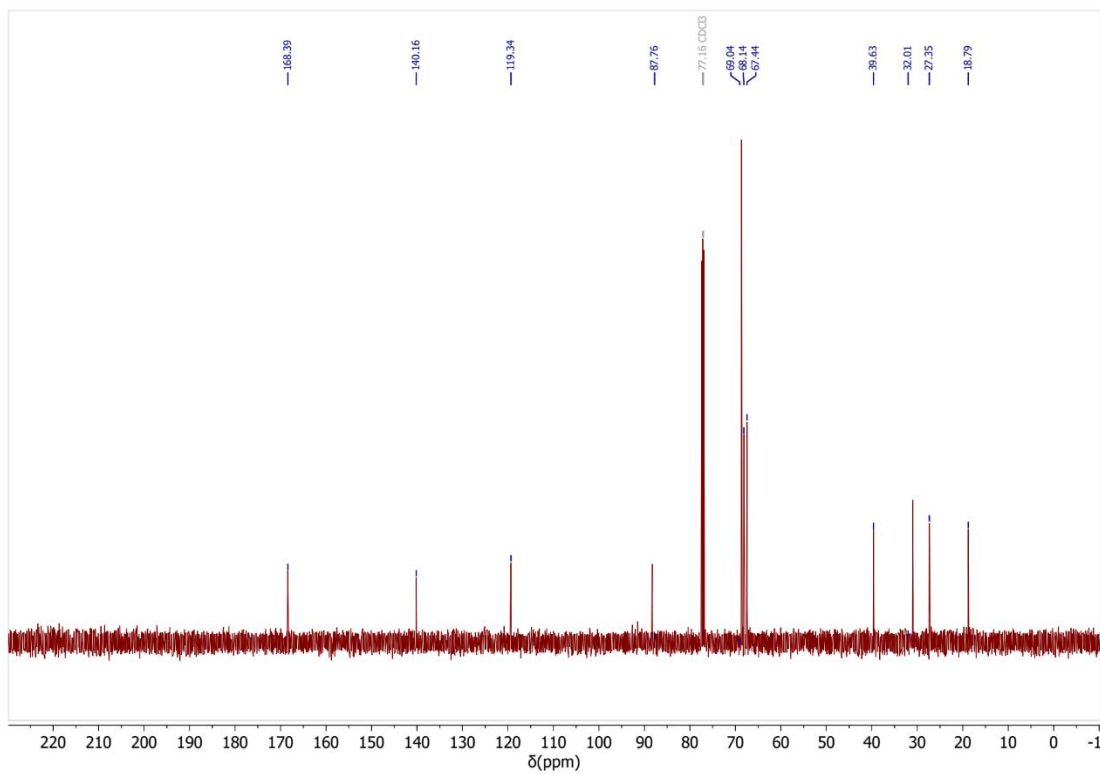


Figure S20. $^{13}\text{C-NMR}$ spectrum of 3-ferrocenyl propyl methacrylamide (FPMAm) (126 MHz, CDCl_3).

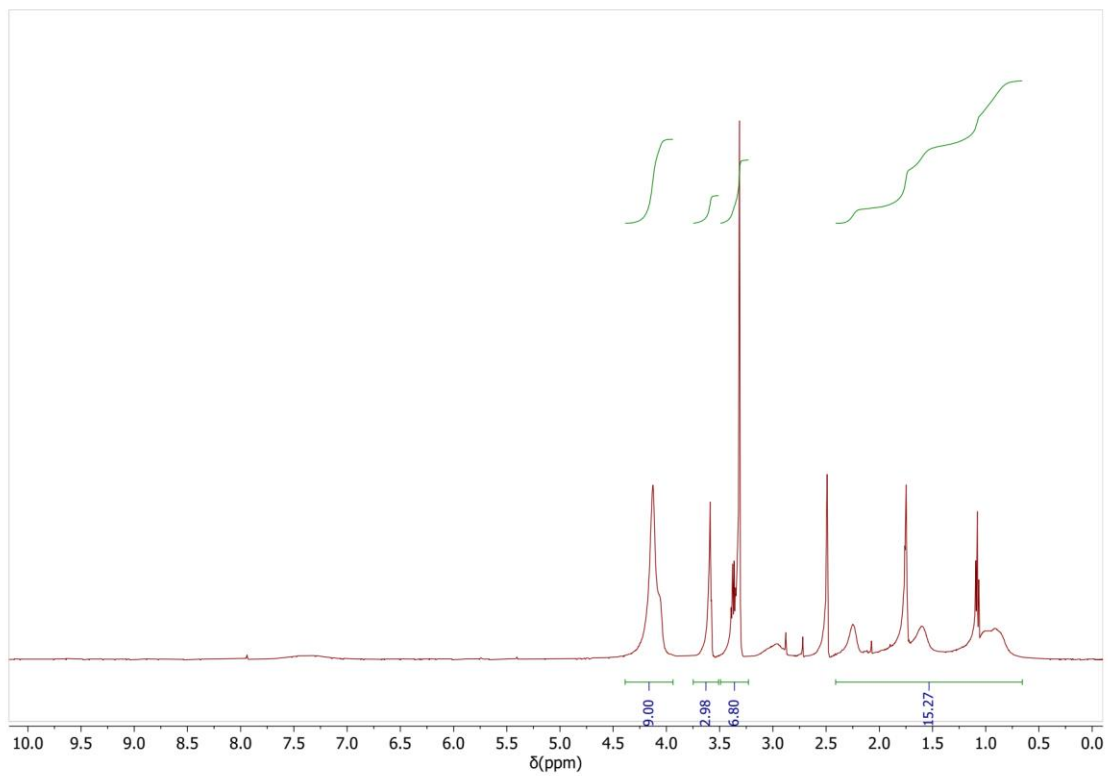


Figure S21. $^1\text{H-NMR}$ spectrum of P1 (500 MHz, $\text{D}_6\text{-DMSO}$).

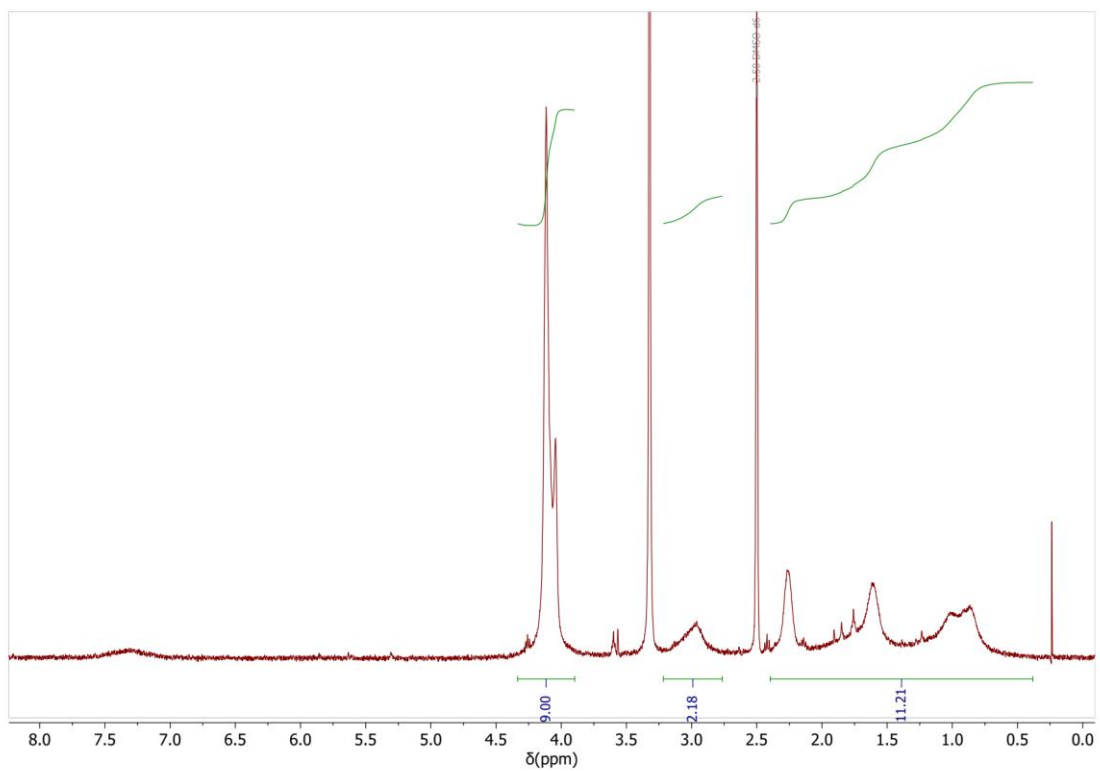


Figure S22. $^1\text{H-NMR}$ spectrum of P2 (500 MHz, $\text{D}_6\text{-DMSO}$).

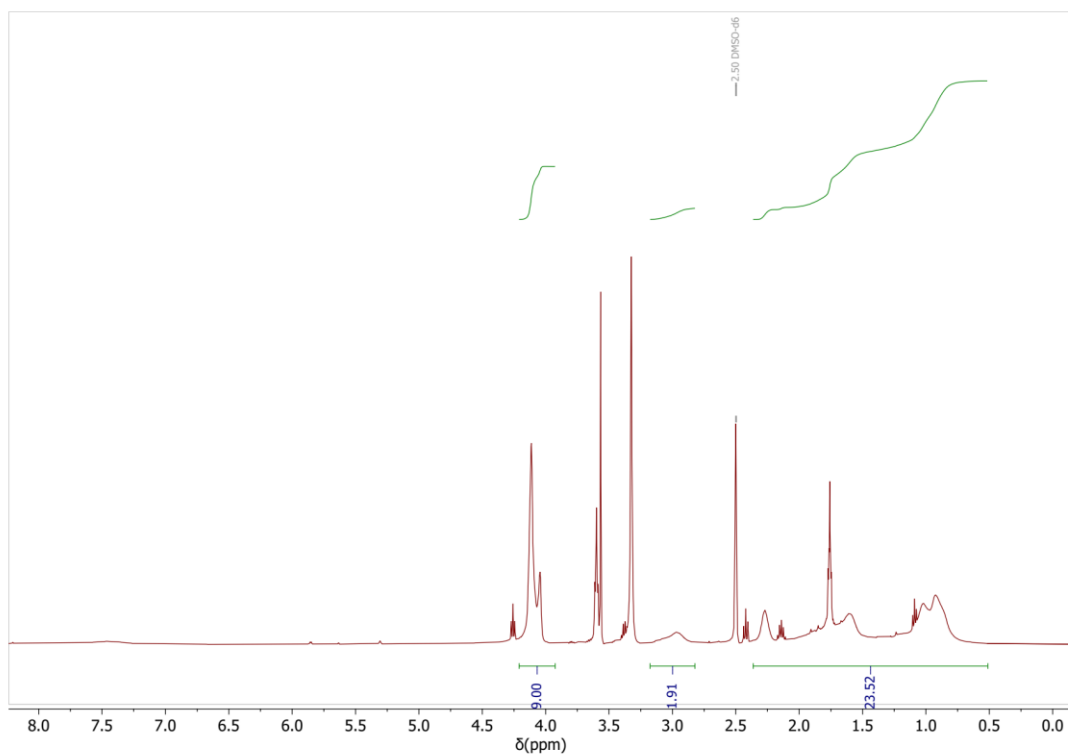


Figure S23. ¹H-NMR spectrum of P3 (500 MHz, D₆-DMSO).

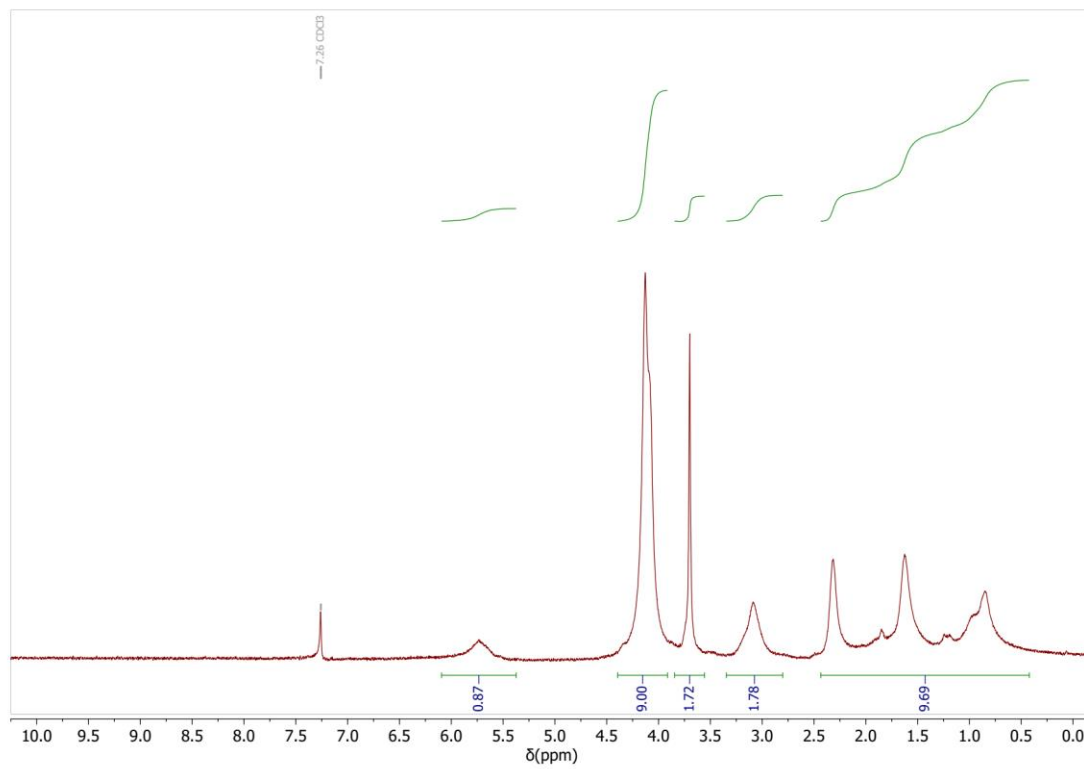


Figure S24. ¹H-NMR spectrum of P4 (500 MHz, CDCl₃).

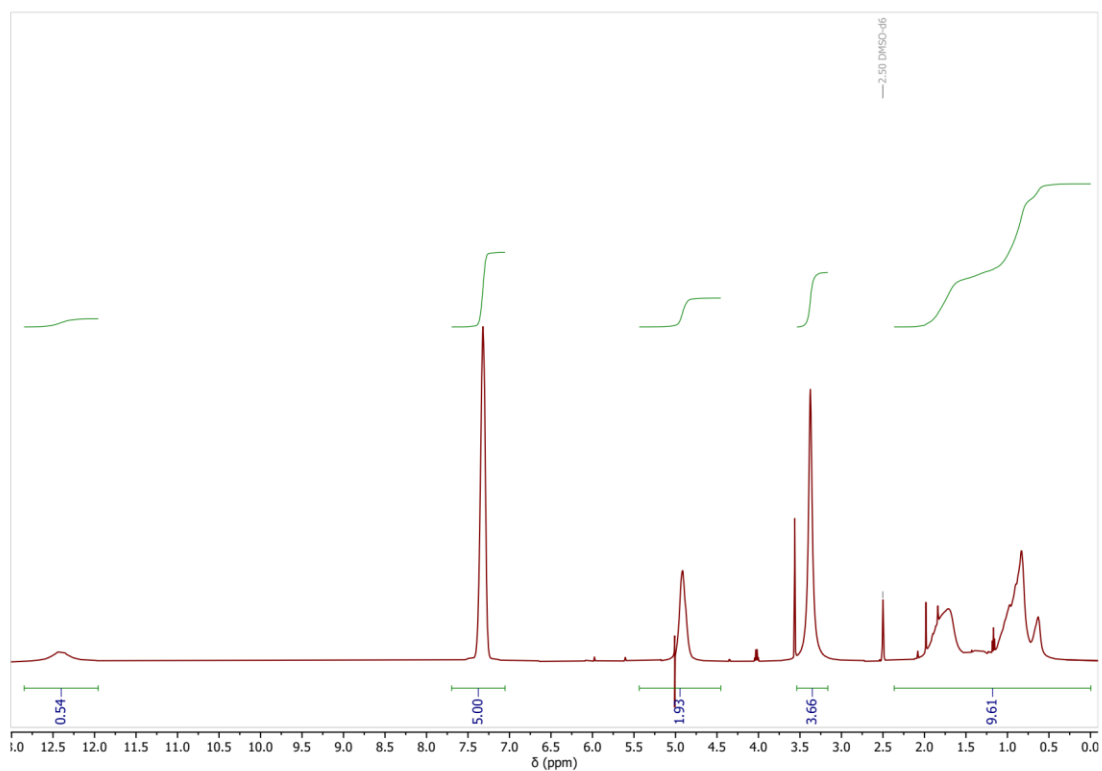


Figure S25. ¹H-NMR spectrum of P5 (500 MHz, D₆-DMSO).

SI-11. P(FPMAm-co-MAA)-CNT electrode cycling: Reduction during uptake stage

Testing cycling if reduction occurred while uptake steps after the first cycle.

Sorption solution: 10 mL of 1 mM YCl₃ / 20 mM NaCl; Sorption solution: 10 mL of 20 mM NaCl

Sorption conditions:

Cycle 1: 1 h open circuit

Cycle 2-3: 1 h chronopotentiometry -0.025 mA

Desorption conditions:

Cycle 1-3: 1 h chronoamperometry 0.8 V vs Ag/AgCl

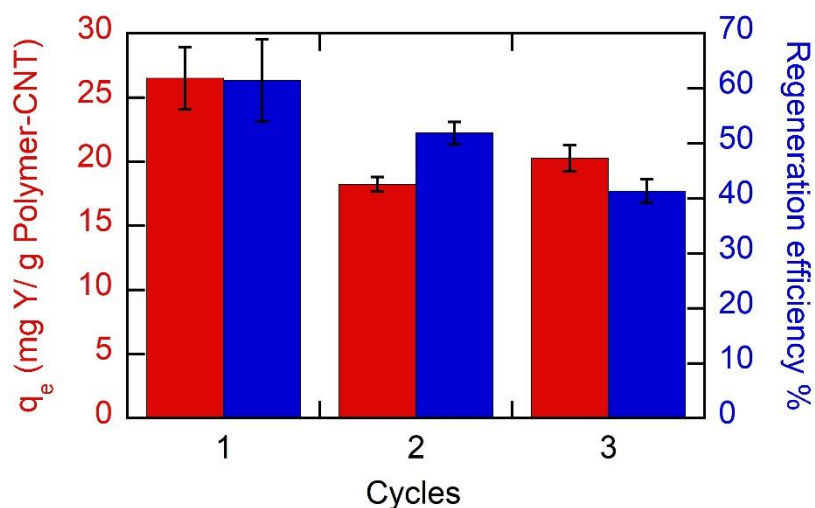


Figure S26. P1-CNT/Ti cycling for Y recovery. Reduction during uptake.

SI-12. P(FPMAM-co-MAA)-CNT electrode desorption energy consumption

$$\text{Energy Consumption (J)} = \int (\text{Potential (V)} \times \text{Current (A)})$$

Energy consumption per desorbed moles of Y for P1-CNT Electrode Desorption first cycle (1 h at 0.8 V vs Ag/AgCl):
331.62 kJ/mol Y (79.2 kcal/mol Y)

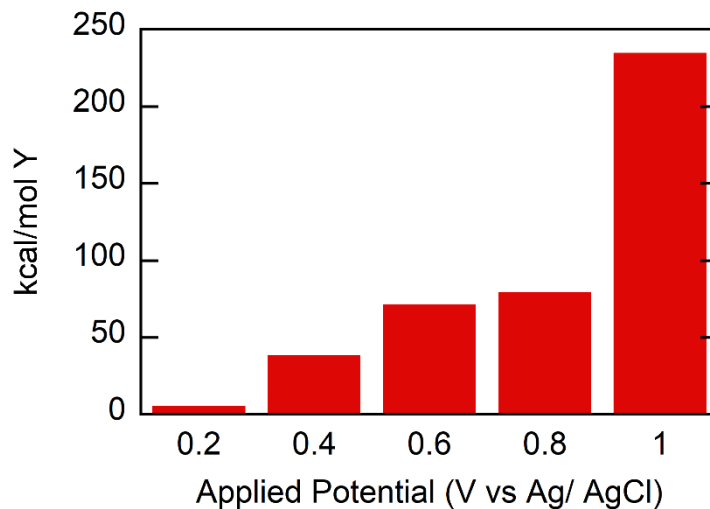


Figure S27. Energy consumption per desorbed moles of Y at various desorption potentials

SI-13. Gel Permeation Chromatography (GPC)

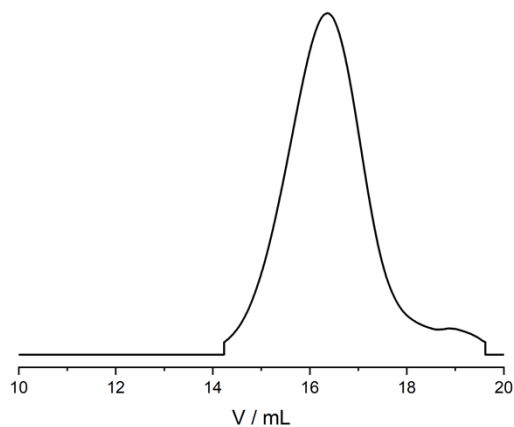


Figure S28. Elugram of the size-exclusion-chromatography of P(FPMAM₆₉-co-MAA₃₁) (P2).

SI-14. Dynamic Light Scattering

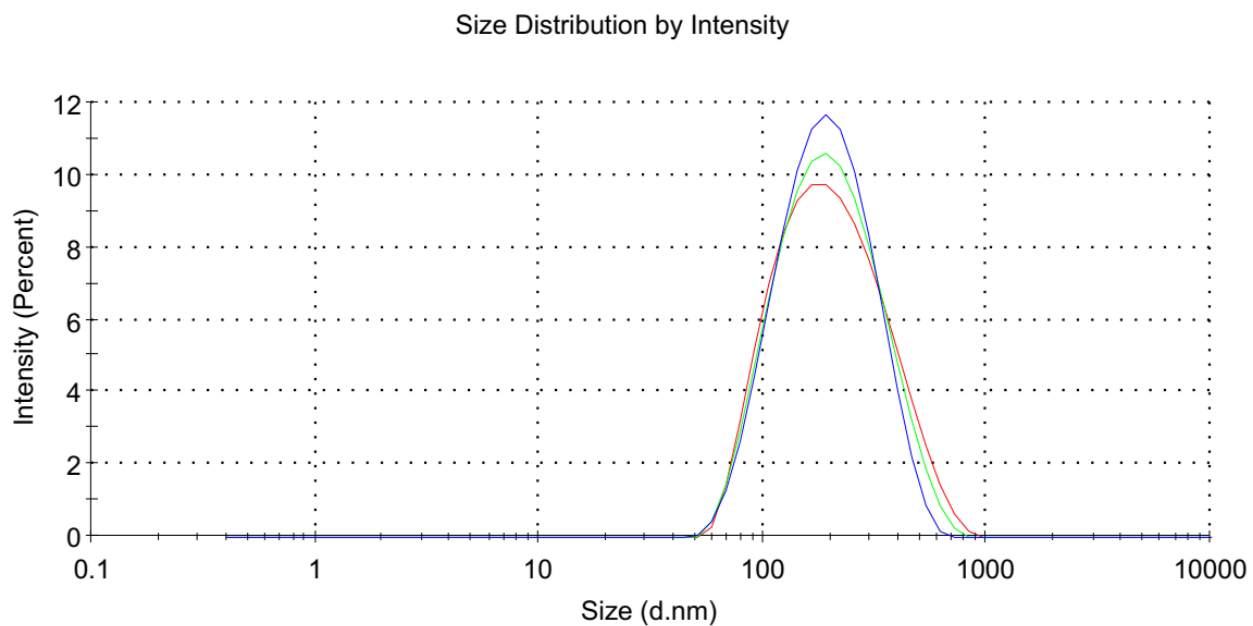


Figure S29. Intensity weighted size distribution of P(FPMAM₄₄-co-MAA₅₆) (P1) in DMF measured by DLS.

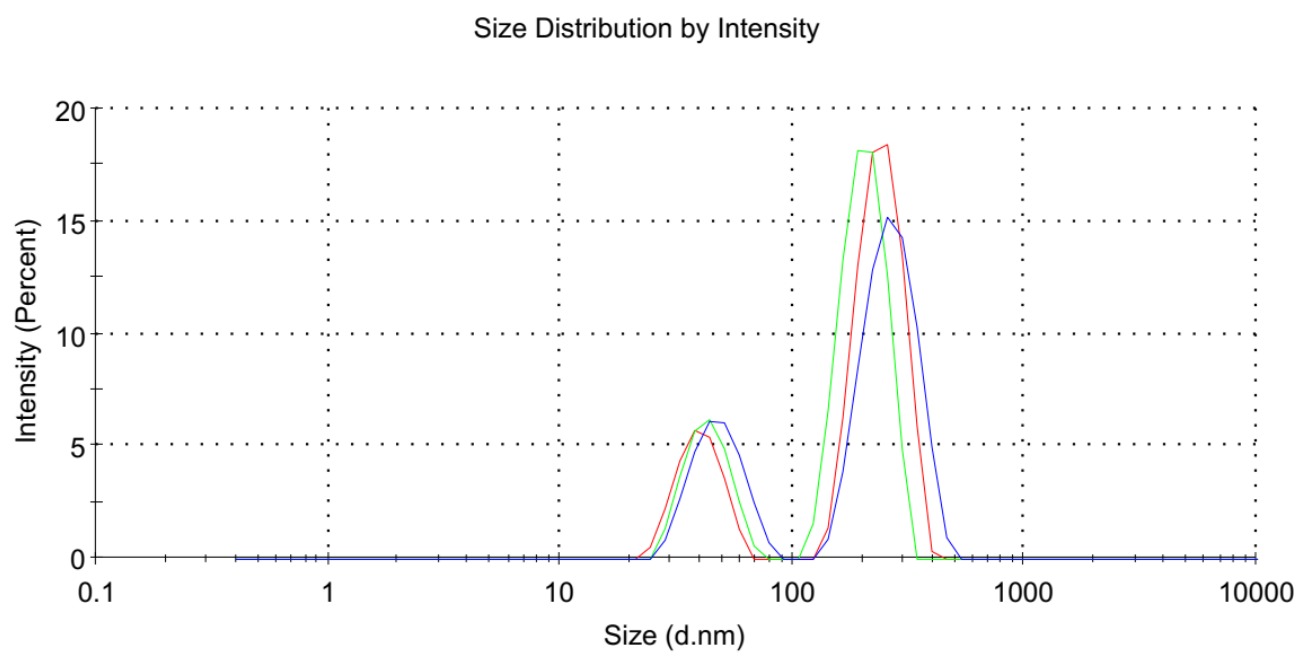


Figure S30. Intensity weighted size distribution of P(FPMAm₄₄-co-MAA₅₆) (P1) in water measured by DLS.

SI-15. Effect of ionic strength on adsorption

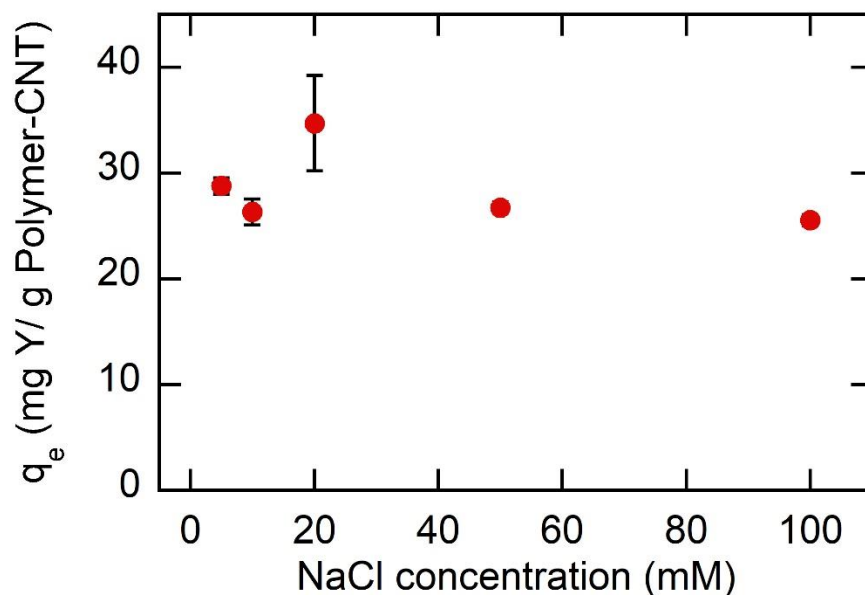


Figure S31. Effect of ionic strength on Y(III) adsorption uptake on P1-CNT.

SI-16. Adsorption of Y from water using different adsorbents

Table S4. Comparison of Y adsorption capacity and regeneration method of different adsorption materials (table adopted from¹⁰).

Adsorbent	Uptake / mg Y/g adsorbent	Regeneration	Ref
P(FPMAm-co-MAA)/CNT	69.4	Electrochemical	This work
SiO ₂ /AC/APTES(PAN) NC	84.1	1 M HNO ₃	11
3D GO/MA NC	16.96	0.1 M HCl	12
3D GO/CZ NC	14.2	2 M HNO ₃	13
3D GO/EW NC	32.16	0.1 M HNO ₃	14
3D GO/HGF NC	32.84	0.1 M HNO ₃	15
Fe₃O₄(CA) NPs	35.8	0.5 M HNO ₃	16
Fe ₃ O ₄ (Cys) NPs	13.6	0.1 M HNO ₃	17
Fe ₃ O ₄ @mSiO ₂ -DODGA NPs	16.29	0.01 M EDTA	18
Fe ₃ O ₄ /SiO ₂ (P507) NC	7.3	0.67 M HCl	19
γ -Fe ₂ O ₃ NP	13.5	Irreversible adsorption	20

SI-17. Adsorption concentration changes

Looking at concentration changes of Y with copolymers of various ratios of ferrocenyl groups to carboxylic acid groups along with CNT/Ti electrodes and no electrodes (just stirring), the latter denoted as blank.

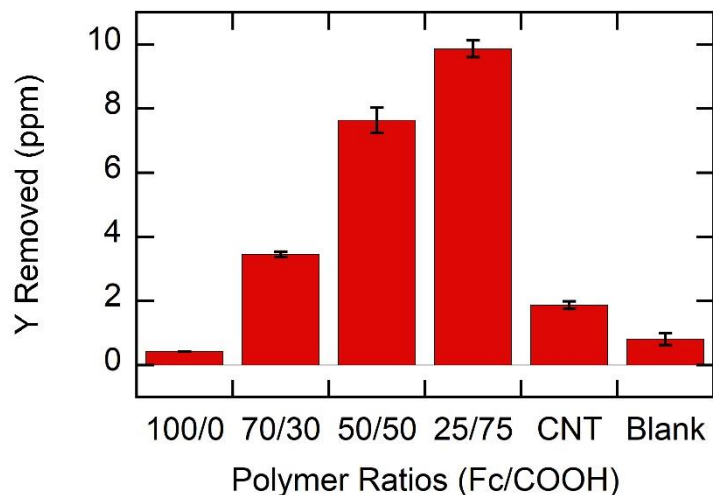


Figure S32. Concentration change of Y(III) onto polymer-CNT/Ti electrodes, with copolymers of various ratios of ferrocenyl groups to carboxylic acid groups along with CNT/Ti electrodes and no electrodes (blank).

SI-18. P(FPMAM-co-MAA)-CNT electrode solution pH changes

Table S5 shows the pH before and after an adsorption/release experiment, for Y adsorption and Y electrochemical desorption, under the standard conditions described in the methodology.

Table S5. Solution pH before and after uptake run and desorption run.

pH	Uptake		Desorption	
	Before Run	After Run	Before Run	After Run
	6.0	5.8	7.2	6.8

SI-19. P(FPMAM-co-MAA)-CNT electrode distribution coefficient

The distribution coefficient K_d was calculated using $K_d = ((C_0 - C) \times V/C)/m$, where C_0 and C are the initial and final REE ion concentration (mg/L), V is the volume of the solution (L), and m is the mass of the electrode coating (g).^{21, 22} In Table S6 we see that the higher the distribution coefficient (K_d) value and adsorption capacity (q) are, the more effective the sorbent material is. Like q , K_d shows that the material is dependent on pH, with better binding at higher pH values.

Table S6. Comparison of Y adsorption capacity (q , mg/g) and distribution coefficient (K_d , mL/g) using P1-CNT/Ti electrodes.

pH	q (mg Y/ g P1-CNT)	K_d (mL/ g P1-CNT)
2	1.5	$6.8 \cdot 10^1$
3	3.0	$1.3 \cdot 10^2$
4	23.6	$1.2 \cdot 10^3$
5	25.7	$1.6 \cdot 10^3$
6	34.7	$2.1 \cdot 10^3$
7	28.3	$1.7 \cdot 10^3$

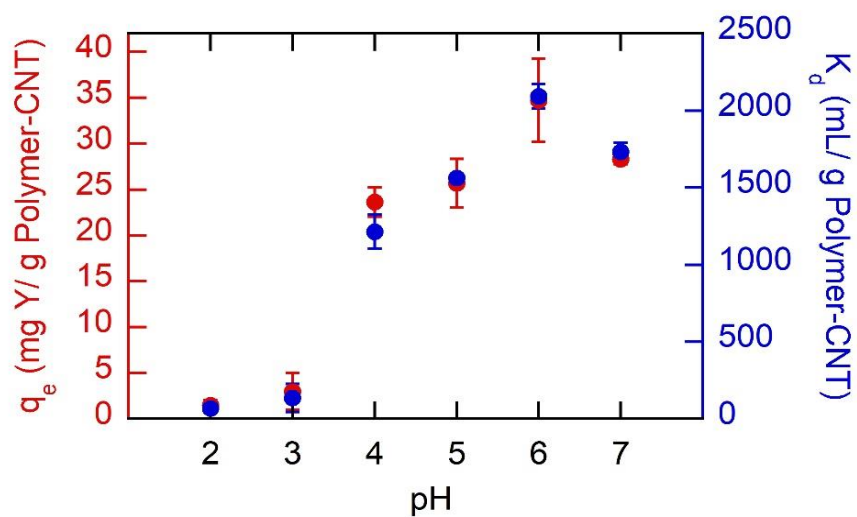


Figure S33. Comparison of Y adsorption capacity (q , mg/g) and distribution coefficient (K_d , mL/g) using P1-CNT/Ti electrodes.

References

1. D. A. Baker, G. C. East and S. K. Mukhopadhyay, *Journal of Applied Polymer Science*, 2001, **79**, 1092-1100.
2. K. Kim, S. Cotty, J. Elbert, R. Chen, C.-H. Hou and X. Su, *Advanced Materials*, 2020, **32**, 1906877.
3. X. Su, H. J. Kulik, T. F. Jamison and T. A. Hatton, *Advanced Functional Materials*, 2016, **26**, 3394-3404.
4. X. Su, J. Hübner, M. J. Kauke, L. Dalbosco, J. Thomas, C. C. Gonzalez, E. Zhu, M. Franzreb, T. F. Jamison and T. A. Hatton, *Chemistry of Materials*, 2017, **29**, 5702-5712.
5. S. Azizian, *Journal of Colloid and Interface Science*, 2004, **276**, 47-52.
6. Z. Wu, H. Joo and K. Lee, *Chemical Engineering Journal*, 2005, **112**, 227-236.
7. I. Langmuir, *Journal of the American Chemical Society*, 1918, **40**, 1361-1403.
8. S. J. Allen, G. McKay and J. F. Porter, *J Colloid Interface Sci*, 2004, **280**, 322-333.
9. H. Moon and W. Kook Lee, *Journal of Colloid and Interface Science*, 1983, **96**, 162-171.
10. T. Kegl, A. Košak, A. Lobnik, Z. Novak, A. K. Kralj and I. Ban, *Journal of Hazardous Materials*, 2020, **386**, 121632.
11. D. L. Ramasamy, V. Puhakka, E. Repo, S. Ben Hammouda and M. Sillanpää, *Chemical Engineering Journal*, 2018, **341**, 351-360.
12. X.-R. Zhao, X. Xu, J. Teng, N. Zhou, Z. Zhou, X.-Y. Jiang, F.-P. Jiao and J.-G. Yu, *Ecotoxicology and Environmental Safety*, 2019, **176**, 11-19.
13. X. Xu, X.-Y. Jiang, F.-P. Jiao, X.-Q. Chen and J.-G. Yu, *Journal of the Taiwan Institute of Chemical Engineers*, 2018, **85**, 106-114.
14. X. Xu, J. Zou, X.-R. Zhao, X.-Y. Jiang, F.-P. Jiao, J.-G. Yu, Q. Liu and J. Teng, *Colloids and Surfaces A: Physicochemical and Engineering Aspects*, 2019, **570**, 127-140.
15. X. Xu, J. Zou, J. Teng, Q. Liu, X.-Y. Jiang, F.-P. Jiao, J.-G. Yu and X.-Q. Chen, *Ecotoxicology and Environmental Safety*, 2018, **166**, 1-10.
16. R. M. Ashour, R. El-sayed, A. F. Abdel-Magied, A. A. Abdel-khalek, M. M. Ali, K. Forsberg, A. Uheida, M. Muhammed and J. Dutta, *Chemical Engineering Journal*, 2017, **327**, 286-296.
17. R. M. Ashour, A. F. Abdel-Magied, A. A. Abdel-khalek, O. S. Helaly and M. M. Ali, *Journal of Environmental Chemical Engineering*, 2016, **4**, 3114-3121.
18. J. Li, A. Gong, F. Li, L. Qiu, W. Zhang, G. Gao, Y. Liu and J. Li, *RSC Advances*, 2018, **8**, 39149-39161.
19. S. Qiu, Z. Zhao and X. Sun, *Journal of Chemical & Engineering Data*, 2017, **62**, 469-476.
20. S. S. Dubey and S. Grandhi, *Journal of Environmental Chemical Engineering*, 2016, **4**, 4719-4730.
21. G. E. Fryxell, Y. Lin, S. Fiskum, J. C. Birnbaum, H. Wu, K. Kemner and S. Kelly, *Environmental Science & Technology*, 2005, **39**, 1324-1331.
22. D. Sheng, L. Zhu, C. Xu, C. Xiao, Y. Wang, Y. Wang, L. Chen, J. Diwu, J. Chen, Z. Chai, T. E. Albrecht-Schmitt and S. Wang, *Environmental Science & Technology*, 2017, **51**, 3471-3479.